Supporting Information

I. Monte-Carlo simulation

I.1 Spectrum of Tungsten X-ray

The x-ray spectrum for a 100-kVp tungsten source is taken from Tucker et al with 1 keV increments and normalized to 60 sec exposure at 3.21×10^{10} photons/cm^2/sec.[1]

I.2 X-ray Absorption and Auger Process in Gold

The tungsten spectrum is weighted by the photoelectric cross-section of gold to obtain the number of photons being absorbed:

$$I_{absorbed} = I_o \sigma N \quad (1)$$

where I_o is equal to the flux of photons hitting the nanoparticle, σ is the photoelectric cross-section, and N is the number of atoms per nanoparticle. The new spectrum is then normalized to produce an array of electrons to be processed discretely via the Monte Carlo method. The simulation closely resembles that of Pomplun et al.[2] For an absorbed photon of a given energy, a hole is produced based on the probabilities of Scofield,[3] and is accompanied by an ejected photoelectron with energy equal to the difference between the incoming photon energy and the binding energy. This shell is then allowed to undergo LMN Auger process, where L is the original vacancy shell, M is the shell from which another electron comes to fill the vacancy, and N is the shell that produces the ejected Auger electron. As a result, this process produces two new vacancies. The transition probabilities for the LMN transition are taken from Chen et al and McGuire.[4] The energy of the Auger electron is assigned as:

$$E_{auger} = (E_M - E_L) + E_N \quad (2)$$

where E is the binding energy of the respective shells. This process is allowed to iterate until the vacancy reaches the N shell, producing an Auger electron each time. Because of the absence of Auger data on outer shells, the iteration is terminated after the N shell. In the case of x-ray fluorescence, which is only modeled for K and L shell vacancies (the two most probable vacancies for producing fluorescence), the fluorescence yield was used to predict whether the hole undergoes fluorescence or the Auger process. A random number between 0 and 1 was generated, and if less than the fluorescence yield, fluorescence occurs. Fluorescence is modeled by:

$$h\upsilon = E_L - E_M \quad (3)$$

where E_L and E_M designate the binding energy of the incident and vacancy shells, and $h\upsilon$ signifies the energy of the photon being generated. The energies of the Auger electrons are stored into an array that is used in the electron transport code for modeling the transport through the nanoparticle or nanotubule.

I.3 Electron Transport through Gold

Electrons are assumed to be generated from an atom randomly chosen in a nanoparticle or nanotubule. The distance it travels before an interaction is given by:

$$L = \lambda_{total} \ln R \quad (4)$$

Energy loss is calculated according to:

$$E_{n+1} = E_n + L\frac{dE}{ds} \quad (5)$$

where λ is the total mean free path, calculated by:

$$\frac{1}{\lambda_{total}} = \frac{1}{\lambda_{elastic}} + \frac{1}{\lambda_{inelastic}} \quad (6)$$

and R is a random number between 0 and 1. The inelastic mean free path for gold are taken from the database of inelastic mean free path from NIST[5] and the elastic mean free path is calculated by:

$$\lambda_{elastic} = \frac{1}{n\sigma_{elastic}} \quad (7)$$

where n is the number density of gold and $\sigma_{elastic}$ is the elastic cross-section taken from NIST.[6] dE/ds in Eq. (5) is the modified Bethe equation given by Joy et al:[7]

$$\frac{dE}{ds} = \frac{-785\rho Z}{AE}\ln\left[\frac{1.166\,(E+kJ)}{J}\right] \quad (8)$$

where ρ is the density (in g/cm^3), Z is the atomic number, A is the atomic weight, E is the energy (in eV), and J is the mean ionization potential of the material (in eV). k is a proportionality constant, which is .851 for gold.[7] A random number is chosen, and the type of scattering is determined through the relative weights of the cross sections in a probabilistic fashion. If it is less than $\sigma_{elastic}/(\sigma_{elastic}+\sigma_{inelastic})$, then an elastic scattering occurs; If it is greater, than an inelastic scattering occurs. If it is an elastic collision, the electron simply changes directions according to the differential cross-section provided by NIST.[6] A random number between 0 and 1 is chosen and from this number, the angle can be obtained by solving for θ:

$$R = \frac{\int_0^{\theta} \frac{d\sigma}{d\theta} d\theta}{\int_0^{\pi} \frac{d\sigma}{d\theta} d\theta} \tag{9}$$

where R is the random number and $d\sigma/d\theta$ is the differential cross-section. The angle is then converted into the azimuthal and polar angles in laboratory coordinates according to Williamson and Duncan.[8] The next position of the electron in Cartesian coordinates is given as:

$$\begin{pmatrix} x_{n+1} \\ y_{n+1} \\ z_{n+1} \end{pmatrix} = \begin{pmatrix} x_n \\ y_n \\ z_n \end{pmatrix} + s_n \begin{pmatrix} \sin\theta_n \cos\phi_n \\ \sin\theta_n \sin\phi_n \\ \cos\theta_n \end{pmatrix} \tag{10}$$

where S_n is the path length, x_n, y_n, z_n is the initial coordinate, θ_n and φ_n are the azimuthal and polar angles. This process continues until the electron exits the boundaries of the nanoparticle. Figure SI.I.3 shows the results.

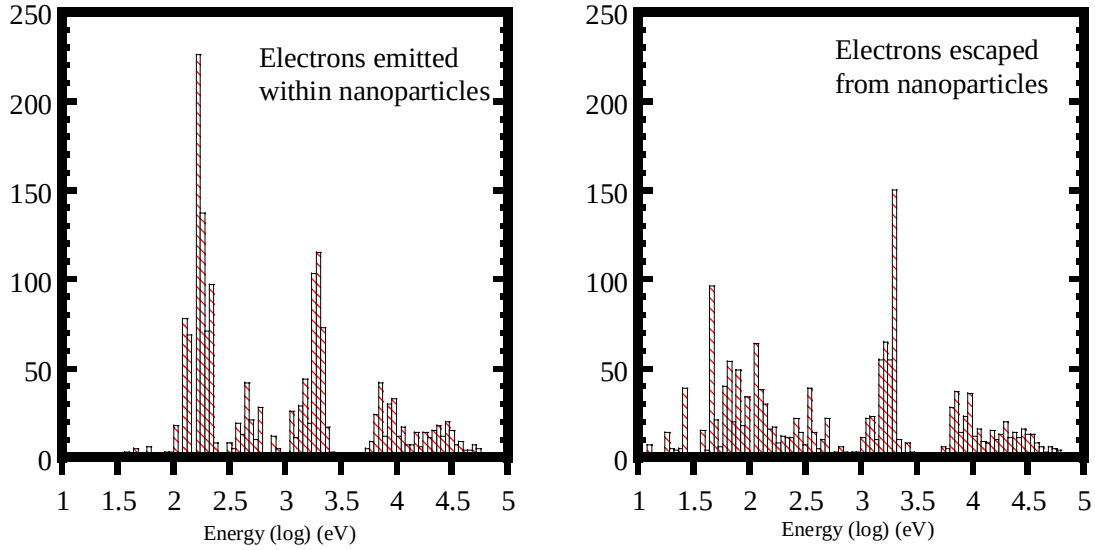

Figure SI.I.3. Monte-Carlo simulation of electrons generated from and escaped a 3-nm gold nanoparticle (top two panels). The absorbing atom was chosen randomly in the nanoparticle. Left panels show the electrons emitted from the gold atoms, and right panels show the electrons escaping the nanoparticles. Low energy electrons (0-100 eV) start to decrease (70%) for 4-nm nanoparticles and become much less (10%) for 5-nm gold nanoparticles.

I.4 Transport of Electrons in Water

The length of electron travel is determined according to Eq (4). The energy loss for sub-keV electrons is taken from the stopping power given by Pimblott et al.[9] The new energy is calculated using a one-angstrom increment. At the end of the path, the electron undergoes elastic scattering. Energy loss due to inelastic scattering was taken into account by the stopping power, and therefore not discretely modeled. For electrons with energies below 1 keV, the differential elastic scattering cross-section is taken from Katase et al.[10] The cross-sections are obtained at 100, 200, 300, 400, 500, 700, 1000eV. At energy intervals, the cross-section corresponding to the nearest energy is used to simulate the scattering. Elastic scattering was not modeled for energies higher than 1 keV due to the lack of experimental data. Fortunately, because the elastic cross-section decreases by an order of magnitude when the scattering angle changes from 0 to 20 degrees even for 1 keV electrons, we assume that the scattering angle to be negligibly small at energies greater than 1 keV. The electron is then iterated until the energy is less than 25 eV.

I.5 Generation of Compton Electrons in Water

In water, a Compton scattered photon would generate a Compton electron. The energy of this Compton electron is calculated by the differential cross-section given by:

$$\frac{d\sigma}{dE} = S(x, Z) \frac{d\sigma}{dE}_{Klein-Nishina} \tag{11}$$

where S(x,Z) is the incoherent scattering function given in Hubbell et al for oxygen, given the absence of the incoherent scattering function for water.[11] $d\sigma/dE_{Klein\text{-}Nishina}$ is the Klein-Nishina differential cross-section given by:[12]

$$\left(\frac{d\sigma}{d\Omega}\right)_{fC} = \left(\frac{{r_0}^2}{2}\right)\left(\frac{k_c}{k_o}\right)^2\left(\frac{k_c}{k_0}+\frac{k_0}{k_c}-\sin^2\theta\right) \quad (12)$$

$$k_c = \frac{k_0}{1+\frac{k_0}{{m_0c}^2}(1-\cos\theta)} \quad (13)$$

$$x = \frac{k_0}{12.399}\sin\left(\frac{\theta}{2}\right) \quad (14)$$

where r_o is the classical electron radius, k_o and k_c are the incident and Compton-scattered photon energies (in keV) for an electron at rest. θ is the scattering polar angle, x is the momentum transfer (in $Å^{-1}$). A random number is chosen and the energy can be obtained by:

$$R = \left(\int_0^E d\sigma/dE \; dE\right) \times \left(\int_{E\min}^{E\max} d\sigma/dE \; dE\right) \quad (15)$$

This process is iterated for all the photons undergoing Compton scattering. Multiple scattering was not considered in our simulation.

I.6 Photoelectron Generation in Water

In an approximation the photoelectron energy is obtained by subtracting the photon energy from the binding shell of the $2a_1$ molecular orbital, which has a binding energy of 30.9 eV.[13] The $1a_1$ molecular orbital is not easily accessible, as shown by Katase et al. and therefore not considered in our photoionization process.[10]

I.7 Electron Spectrum in Water

Electrons generated in water are different from electrons interacting with nanoparticles. The former can be simply calculated based on the absorption cross-sections of Compton electrons and photoelectrons. Figure SI.I.7 shows the results.

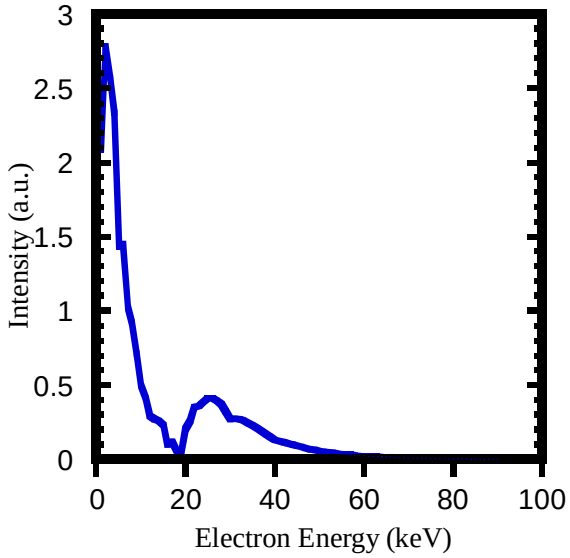

Figure SI.I.7. Energy distribution of all the electrons (including Compton electrons and photoelectrons) generated in pure water. The low-energy electrons are generated through Compton scattering, and the high-energy electrons from photoelectric effect.

We can then estimate the energy profile of electrons in water that can reach a gold nanoparticle by summing up the total number of electrons traversing through a volume element per unit time. The Compton electrons (normally with less than 10-keV energy) are summed up to 10 μm sphere in 10 nm increments. For each increment, the profile of Compton electrons generated is simulated to travel the respective distances. The energy loss is predicted by the stopping power mentioned earlier.[9] The energies were chosen to be statistically representative of the Compton profile of water. The photoelectrons are summed up to 70 μm in 100 nm increments using the same method. The ratio of Compton and photoelectrons is determined by the corresponding absorption cross-sections.

I.8. Fraction of Electrons Colliding with the Nanoparticle

Given a spherical volume of water, it is necessary to calculate the number of electrons impinging upon a nanoparticle. Using the simulation above, the transport of electrons in water is simulated. The fraction of the electrons emitted toward the nanoparticle is given by:

$$N = \int_{volume} \lambda(R)\rho \, dV \tag{16}$$

where ρ is the electron density generated in water and λ is the fraction of electrons that will hit the nanoparticle, assuming that the electrons are emitted in an isotropic fashion. This is equivalent to the fractional area of the nanoparticle

$$N = \int_0^R \frac{\pi R_{NP}^2}{4\pi r^2} \rho r^2 dr \sin\theta \, d\theta \, d\vartheta = \pi R_{NP}^2 R \rho \tag{17}$$

where R is the estimated maximum penetration depth of the electrons, which are chosen to be 10 and 70 μm in the Compton and photoelectron case, respectively.

I.9 Absorption of the Electrons by the Nanoparticle

The number of electrons that undergo ionization through interaction with the gold nanoparticle was calculated using the differential ionization cross-section given by Vriens and Møller et al.,[14] similar to that by Yasuda et al.[15] The inner shell ionization uses Vriens differential cross-sections while the outer shell excitation uses Møller's. The total ionization cross-section is then obtained. The total number of electrons absorbed is obtained by applying the calculated cross sections to equation 1. The energy transfer to the secondary electron generated through the same method as Eq. (10). Taking into account the binding energy, the energies of the primary and secondary electrons are calculated.

I.10 Energy Deposition in Water

The simulation is performed using the same methodology described in I.4. The energy deposition rate is calculated via the stopping power from Pimblott.[9] The energy density (energy divided by volume) deposited is plotted as a function of distance from the nanoparticle. The average energy density per spherical shell is plotted as a function of distance from the nanoparticle.

I.11 Calculation of Enhancement

The energy deposited by the nanoparticle is calculated by using a statistical representation of 969 electrons taken from the end result of I.3 and I.9. This sample is inputted into the program described in I.10.

The average energy density of radicals is calculated in the manner as described: First, The cross-section of photoelectric absorption and Compton scattering is used to obtain the number of respective electrons generated per unit volume. Given our assumption that the outward flux of electrons is approximately equivalent in number and energy to the ones coming in, the entirety of the electron energy is deposited locally. Using the number of Compton electrons and Photoelectrons and their respective average energies, the total energy deposition within the cube is calculated.

Given a DNA of a length of 500 nm, on average the nanoparticle spacing will be 50 nm. The enhancement is calculated by taking the ratio of the energy deposited by the electrons from the nanoparticle versus the integration of the average energy density of radicals in water within a 50 nm cylinder of water around the DNA and plotting as a function of cylindrical radius. In this model, the non-linearity of DNA is not taken into account.

I.12 Radical Diffusion and the effect of Tris on the Average Diffusion Distance of Hydroxyl Radicals

Diffusion of the hydroxyl radicals is modeled using the second Fick's diffusion law. The simulation method is identical to the one used by Kuppermann et al.[16] A Gaussian spur of 1 hydroxyl radicals is generated and allowed to react using the simulation method described above. Diffusion was modeled and considered terminated till the distribution decays to only 5% of the initial concentration. The average diffusion distance for each time-step is calculated by taking the average of the final positions of the radicals.

For the reaction of radicals from water with DNA, a homogeneous radical concentration equivalent to that generated from 1-Gy absorbed radiation was modeled around DNA. Radical recombination, Tris base scavenging, and reactions with DNA were modeled using the kinetics rate law. DNA-radical interactions only occur within the volume defined by the reaction radii of the DNA. The number of radicals reacting with the DNA is related to the single strand break yield with an efficiency of 25% given by Milligan et al.[17] The quantity is then calibrated to the %DNA damage/Gy (absorbed radiation), assuming that a strand break per DNA results in 100% damage (i.e., conversion from supercoiled to circular DNA).

II. Sample preparation and radiation experiments

II. 1 Preparation of $CH_3(OCH_2CH_2)_3SH$:

Following a synthetic scheme established by Foos and co-workers,[18] we synthesized 2-[3-(2-Methoxy-ethoxy)-propoxy]-ethanethiol. Briefly, tri(ethylene glycol) monomethyl ether (5.0 g, 30.4 mmol) was dissolved in 12 ml of pyridine and cooled to 0 °C. *p*-Toluenesulfonyl chloride (5.8 g, 30.4 mmol) in 12 ml of pyridine was added dropwise under N_2. The reaction was stirred for 2.5 hours, sealed, and stored at 2 °C overnight. The mixture was then added to 120 ml of ice water and stirred for 1 h. From this solution the tosylate was extracted with CH_2Cl_2, dissolved in a minimum amount of ethanol, and transferred to a flask to which thiourea (2.32 g, 30.4 mmol) dissolved in 15 ml of H_2O was then added. The reaction was refluxed for 2 hours at which point NaOH (1.34 g, 33.5 mmol) in H_2O was then added, and reflux continued for 1.5 hours. The solution was then cooled to room temperature, concentrated, and neutralized with HCl. The product was extracted from this aqueous solution with CH_2Cl_2 and isolated as a yellow oil producing 2.84 g of thiol (52% overall yield).

II.2. Preparation of scDNA:

Supercoiled DNA (ϕX174 RF DNA) purchased from Invitrogen was used as received without further processing unless noted otherwise.

II.3 Preparation of Ethidium Ligand:

We synthesized an ethidium-capped thiol ligand for nanoparticle/DNA conjugation using a procedure modified by Wang et al.[19] Briefly, 3,8-diamino-6-phenyl phenanthridine (1.04 g, 3.6 mmol) was dissolved in 7 ml of dry pyridine. To the rapidly stirred mixture ethyl chloroformate (0.75 ml, 7.8 mmol) was added dropwise and allowed to react for 5 h. 100 ml of deionized water was added and the resulting precipitate was collected and purified by recrystallization in aqueous methanol (90% MeOH, 10% H_2O). In a separate reaction, Poly(4-vinylpyridine) (220 mg, 2 mmol) was added to 5 ml methylene chloride followed by addition of trifluoromethane sulfonic anhydride (283 mg, 1.0 mmol). To the rapidly stirred mixture 1-bromoundecanol (238 mg, 0.95 mmol) in 5 ml methylene chloride was added dropwise over 1 minute. The reaction was allowed to proceed for 5 minutes, at which point the precipitate was filtered under gravity and discarded. The filtrate was washed with 10 ml sat. sodium bicarbonate, dried with magnesium sulfate, and concentrated. The resulting 11-bromoundecyl triflate was used without further purification. Alkylation of 3,8-Bis-(ethoxycarbonylamino)-6-phenylphenanthridine (0.429 g, 1 mmol) with the 11-bromoundecyl triflate (0.383 g, 1 mmol) was done in methylene chloride with rapid stirring for 10 hours at room temperature. The resulting 11-bromo-undecyl)-3,8-bis-ethoxycarbonylamino-6-phenyl-phenanthridinium was purified using column chromatography (9:1 $CHCl_3$: MeOH). The pure product was then dissolved in 50 ml methylene chloride and washed with 100 ml of 1 M HBr (4×). The organic layer was collected and concentrated and then refluxed for 18 hours in 10ml 48% HBr. The acid was removed under vacuum and purified by column chromatography (9:1 $CHCl_3$: MeOH) to give 53 mg of red solid.

II.4 Preparation of Charge-Neutral Water-Soluble Gold Nanoparticles:

Following a synthetic scheme established by Foos et al,[18] we synthesized triethylene oxide functionalized gold nanoparticles. In a typical synthesis, $HAuCl_4 \cdot 3H_2O$ (0.7753 g; 1.97 mmol) was dissolved in 63 ml of 18 MΩ H_2O, and added to a rapidly stirred solution of tetraoctylammonium bromide (4.70 g; 8.60 mmol) in 167 ml of toluene. After 5 minutes, hexanethiol (94.7 μl, 0.0782 g; 0.66 mmol) was added to the mixture and allowed to mix for 10 minutes at which point $NaBH_4$ (0.7973 g; 21.1 mmol) dissolved in 52.5 ml of H_2O was added. The mixture was allowed to stir for 3 hours at which point the organic layer was collected, concentrated to a ~10 ml volume, and combined with 400 ml of MeOH. The mixture was stored overnight at –20°C and the resulting precipitate was collected via centrifugation. After complete drying, 100 mg of hexanethiol-capped nanoparticles was dissolved in 10 ml of toluene. 100 mg of the synthesized $CH_3(OCH_2CH_2)_3SH$ was added to the nanoparticle solution and allowed to stir overnight at room temperature. The solvent was removed and redissolved in 5 ml of toluene. Another 100 mg of $CH_3(OCH_2CH_2)_3SH$ was added and the reaction was again allowed to stir overnight at room temperature. The solvent was then removed under vacuum, and the solid washed with 15 ml of heptane (3×). The black solid was vacuum dried for 3 hours yielding greater than 90 mg of charge-neutral water-soluble gold nanoparticles.

II.5 Preparation of Ethidium-Functionalized Water-Soluble Gold Nanoparticles for DNA Conjugation:

Following the method of Wang et al,[19] we synthesized water-soluble gold nanoparticles functionalized with varying amounts of ethidium ligands. In the synthesis of the ethidium functionalized nanoparticles, 1.37 ml of a 7.3 mg/ml solution of the ethylene oxide functionalized gold nanoparticles was combined with 1.25 ml of a 1 mg/ml solution of ethidium ligand in MeOH. A further 2.86 ml of methanol was added and the reaction was allowed to stir for 2 days. The nanoparticle solution was then dried under vacuum, dissolved in 4 ml of 18 MΩ H_2O, and allowed to undergo dialysis for 3 days in 18 MΩ H_2O.

II. 6 TEM (staining of DNA):

Transmission electron microscopy (TEM, Philips CM120 operated at 80 kV) was used for the examination of the nanoparticles and nanoparticle/DNA conjugates. The DNA/nanoparticle conjugates were stained using a method adapted from Hayat.[20] Carbon stabilized formvar coated Copper grids (Ted Pella No. 01801) were floated (specimen side down) on a 10^{-5}% solution of benzalkonium chloride in water overnight. The grids were removed from the solution and the excess was wicked away using filter paper. 5 µl of specimen solution (DNA/nanoparticle conjugates 5 ng DNA/µl in water) was then deposited on the grid for 2 min. At this point the grids were ready for staining following the method of Gordon and Kleinschmidt.[21] A stock solution of 5 mM uranyl acetate in methanol was diluted 50-fold with acetone. The formvar coated copper grid with DNA/nanoparticle droplets still intact was submersed directly into the staining solution for 15 sec, and briefly rinsed with ethanol. The remaining solution was again wicked away with filter paper and air-dried for 1 hour before TEM analysis.

II.7 Gel Electrophoresis of Nanoparticle/DNA Conjugates:

0.8% Agarose E-gels purchased from Invitrogen were used as received. The gels were run at 45 V for 45 min and inspected with a transilluminator (ChemiDoc XRS, Bio-Rad). Nanoparticle/DNA conjugates were prepared by first diluting stock DNA to 100 ng in 10 µl and then combination of this with 10 µl of appropriate concentrations of nanoparticle in water. The conjugates were micro-pipetted 5× to ensure mixing. The total 20 µl aliquot was then transferred to the gel. In cases where a DNA marker was used, 5 µl of marker (All Purpose Hi-Lo DNA Marker/Mass Ladder from Bionexus, Inc.) was diluted with 15 µl of 18MΩ H_2O.

II.8 NMR Measurements:

Nanoparticle NMR spectra were recorded in deuterated-H_2O on a VNMRS 600 (Varian) spectrometer running at 599.8234805 MHz. Chemical shifts (ppm) are internally referenced to the TMS signal (0 ppm) in all cases. Line-broadening factors of 5 and 10 Hz were used to improve S/N ratio.

II.9 Dialysis Purification:

Dialysis was performed using Spectra/Pore® CE (cellulose ester) molecular porous membrane with a MWCO of 10,000. The sealed membranes containing the nanoparticle solutions were allowed to sit in a gently stirred reservoir of 18 MΩ H_2O while the reservoir water was changed once daily for 3 days.

II.10 Purification by Gel Filtration:

When diluted to the concentrations used in radiation testing, supercoiled DNA (ϕX174 RF DNA) purchased from Invitrogen contained micromolar amounts of Tris-HCl, and trace amounts of EDTA and sodium chloride. In cases where the concentration of these buffers needed to be carefully controlled, the stock buffer provided from Invitrogen was first removed and a known amount of Tris base was then added back into the DNA. To achieve this, a 1 ml disposable syringe was filled with pre-swollen Sephadex G-25 Medium (Amersham Biosciences). It was then spun dry using a centrifuge at 5,000 G for 3 minutes. The DNA was then added to the packed column and centrifuged at 5,000 G while the eluted DNA was collected in an autoclaved 200 µl PCR tube.

II.11 Control Experiment to Verify Scavenging Ability of Tris:

To confirm the radical scavenging properties of Tris base, samples containing various Tris base concentrations (up to 50 mM) and 100 ng of scDNA were radiated with a fixed dose of x-rays and analyzed using gel electrophoresis. Included in the gel were non-radiated controls of both scDNA alone and scDNA in 50 mM Tris base. Samples containing higher concentrations of Tris base were found to be less susceptible to radiation damage than those with lower relative amounts of Tris base. This was attributed to the reduced ability of radicals to diffuse in higher concentrations of Tris. The non-radiated controls showed no damage to the scDNA.

II.12 Gold Nanoparticle Radiation Experiment:

Nanoparticle/scDNA conjugates were prepared by diluting stock scDNA to 100 ng in 5 µl of water and combining this with 10 µl of appropriate concentrations of nanoparticle in water and an additional 5 µl of Tris base in water. The control samples contained the required scDNA and Tris base, but 10 µl of water was added in place of the nanoparticle solution. The solutions were then radiated using an HP Faxitron 43855A and the total 20 µl volume was analyzed using gel electrophoresis.

Figure SI.II.12: A typical gel photo from the radiation of gold nanoparticles with scDNA is shown. Lanes 1-3 represent radiated scDNA controls given the same x-ray dose with increasing Tris concentration from left to right. Lanes 4-6 are the corresponding non-radiated scDNA samples. Lanes 7-9 are the radiated counterparts to lanes 1-3 with scDNA conjugated to gold nanoparticles. Again, lanes 10-12 are the corresponding non-radiated scDNA/gold nanoparticle controls.

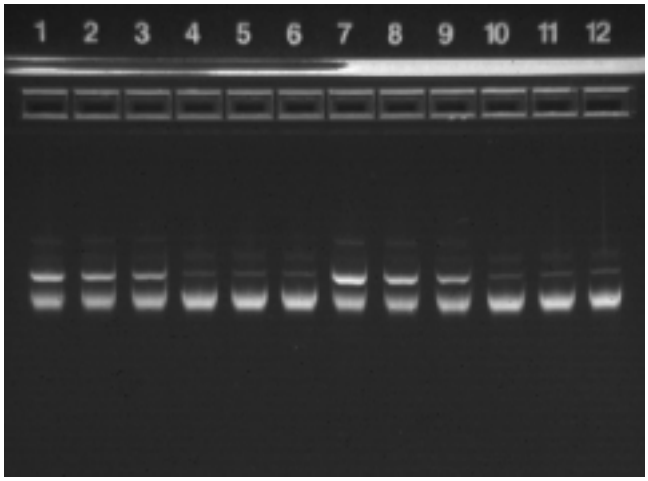

II.13.a Control Experiment to Verify Ethidium-based Ligand Act as a Radiosensitizer:

To ensure the ethidium-based intercalating ligand used to link nanoparticles to scDNA did not act as a radiosensitizer, control experiments were performed. In these experiments, scDNA was added to an aqueous solution of 1.4 µM ligand in 10 mM Tris and given several x-ray doses. The concentration of the ligand was chosen to be 10× the amount present in a typical nanoparticle radiation experiment. In the same experiment, scDNA alone in 10mM Tris and scDNA conjugated to approximately 10 nanoparticles (also in 10 mM Tris) that were given equivalent x-ray doses to the ligand were compared using gel electrophoresis. The nanoparticles showed an enhancement of about 200%, while the scDNA and scDNA with ethidium-based ligand showed an approximately equivalent response to the x-rays. The results demonstrate that the ligand alone is not responsible for the measured enhancement.

II.13.b Control Experiment to Verify Conjugation of Nanoparticles Requirement for X-ray Enhancement:

To verify conjugation of the water-soluble nanoparticles was required in order to see x-ray enhancement, 100 ng of scDNA in 10 µl of water was mixed with water-soluble nanoparticles (missing the Ethidium-based linker ligand) in a ratio similar to that of a typical nanoparticle radiation test (~10 nanoparticles per scDNA). The Tris base concentration was held constant at 10 mM. The samples were given an array of x-ray doses and analyzed using gel electrophoresis. The results of x-ray radiation for the scDNA mixed with non-conjugated gold nanoparticles and scDNA alone were found to be similar, proving the enhancement is present only when the nanoparticles are conjugated to the scDNA.

II.13.c Radiation Test of 5 µM non-conjugated Water-Soluble Gold Nanoparticles with scDNA:

An x-ray enhancement test at near the maximum solubility of water-soluble nanoparticles (~5 µM) was performed. 100 ng of scDNA was mixed with a saturated solution of water-soluble 3 nm gold nanoparticles covered with triethylene glycol (TEG) ligands. No enhancement was observed at any x-ray dose. In some cases, anti-enhancement was observed. Although it is possible to achieve even higher concentrations of gold nanoparticles in the scDNA mixture, the presence of free ligand in these mixtures (increasing with increasing nanoparticle concentrations) would render the chances of x-ray enhancement unlikely.

II.13.d Radiation Test of Reduced Concentration of Gold Nanoparticles with scDNA:

Another control experiment was performed to measure the effect of reducing the number of nanoparticles to 1/3 of the optimized concentration. In this experiment, DNA was first purified of all buffers using sephadex G-25 medium. At this point 5 µl aliquots containing 100 ng DNA were added to twelve 200 µl PCR tubes. Four of these tubes were filled with 10 µl of water as a control experiment, another four were filled with 10 µl gold nanoparticle solution (10:1 ratio of nanoparticles to DNA), and the last four were filled with l0 µl of diluted gold nanoparticles (3.33:1 ratio of nanoparticles to DNA). Finally, all of the samples were filled with 5 µl of 40mM Tris and subsequently mixed. The samples were given varying doses of radiation and compared using gel electrophoresis. The enhancement measured for the diluted nanoparticle samples was approximately 35% of the optimized nanoparticle ratio enhancement.

[1] DM Tucker, GT Barnes, and DP Chakraborty, *Medical Physics* **18** (2), 211 (1991).
[2] E Pomplun, J Booz, and DE Charlton, *Radiation Research* **111** (3), 533 (1987).
[3] J.H. Scofield, *LLNL Rep. UCRL- 52326* (1973).
[4] MH Chen, E Laiman, B Crasemann et al., *Physical Review A* **19** (6), 2253 (1979).

5 National Institute of Standards and Technology, (http://www.nist.gov.srd/nist71.htm).
6 National Institute of Standards and Technology, (http://www.nist.gov.srd/nist64.htm).
7 DC Joy and S Luo, *Scanning* **11** (4), 176 (1989).
8 W Williamson and GC Duncan, *American Journal of Physics* **54** (3), 262 (1986).
9 SM Pimblott, JA LaVerne, and A Mozumder, *Journal of Physical Chemistry* **100** (20), 8595 (1996).
10 A Katase, K Ishibashi, Y Matsumoto et al., *Journal of Physics B-Atomic Molecular and Optical Physics* **19** (17), 2715 (1986).
11 J.H. Hubbell, W.J. Veigele, E.A. Briggs et al., *J. Phys. Chem. Ref. Data* **4** (3), 471 (1975).
12 O Klein and Y Nishina, *Z. Phys.* **52**, 853 (1929).
13 B. Winter, R. Weber, W. Widdra et al., *Journal of Physical Chemistry A* **108** (14), 2625 (2004).
14 L Vriens, *Proceedings of the Physical Society of London* **89** (563P), 13 (1966).
15 M Yasuda, H Kawata, and K Murata, *Journal of Applied Physics* **77** (9), 4706 (1995).
16 A. Kuppermann and G. G. Belford, *Journal of Chemical Physics* **36** (6), 1427 (1962).
17 J. R. Milligan, J. A. Aguilera, and J. F. Ward, *Radiation Research* **133** (2), 151 (1993).
18 E. E. Foos, A. W. Snow, and M. E. Twigg, *Journal of Cluster Science* **13** (4), 543 (2002).
19 G. L. Wang, J. Zhang, and R. W. Murray, *Analytical Chemistry* **74** (17), 4320 (2002).
20 M.A. Hayat, *Principles and Techniques of Electron Microscopy: Biological Applications*. (Van Nostrand Reinhold Company, New York, 1972).
21 CN Gordon and Kleinsch.AK, *Biochimica Et Biophysica Acta* **155** (1), 305 (1968).